

Journal of Maps

ISSN: (Print) (Online) Journal homepage: www.tandfonline.com/journals/tjom20

# The geography of Oxia Planum

**Peter Fawdon, Peter Grindrod, Csilla Orgel, Elliot Sefton-Nash, Solmaz Adeli, Matt Balme, Gabriele Cremonese, Joel Davis, Alessandro Frigeri, Ernst Hauber, Laetitia Le Deit, Damien Loizeau, Andrea Nass, Adam Parks-Bowen, Cathy Quantin-Nataf, Nick Thomas, Jorge L. Vago & Matthieu Volat**

**To cite this article:** Peter Fawdon, Peter Grindrod, Csilla Orgel, Elliot Sefton-Nash, Solmaz Adeli, Matt Balme, Gabriele Cremonese, Joel Davis, Alessandro Frigeri, Ernst Hauber, Laetitia Le Deit, Damien Loizeau, Andrea Nass, Adam Parks-Bowen, Cathy Quantin-Nataf, Nick Thomas, Jorge L. Vago & Matthieu Volat (2021) The geography of Oxia Planum, Journal of Maps, 17:2, 621-637, DOI: 10.1080/17445647.2021.1982035

**To link to this article:** https://doi.org/10.1080/17445647.2021.1982035

© 2021 The Author(s). Published by Informa UK Limited, trading as Taylor & Francis Group.

View supplementary material

Published online: 09 Nov 2021.

Submit your article to this journal

Article views: 2819

View related articles

View Crossmark data

Citing articles: 17 View citing articles

Full Terms & Conditions of access and use can be found at
https://www.tandfonline.com/action/journalInformation?journalCode=tjom20

JOURNAL OF MAPS
2021, VOL. 17, NO. 2, 621–637
https://doi.org/10.1080/17445647.2021.1982035

SCIENCE

OPEN ACCESS Check for updates

# The geography of Oxia Planum

Peter Fawdon [a], Peter Grindrod [b], Csilla Orgel [c], Elliot Sefton-Nash [d], Solmaz Adeli [e], Matt Balme [a], Gabriele Cremonese [f], Joel Davis [b], Alessandro Frigeri [g], Ernst Hauber [e], Laetitia Le Deit [h], Damien Loizeau [i], Andrea Nass [e], Adam Parks-Bowen [j], Cathy Quantin-Nataf [k], Nick Thomas [l], Jorge L. Vago [d] and Matthieu Volat [l]

[a]School of Physical Sciences, Open University, Milton Keynes, UK; [b]Department of Earth Sciences, Natural History Museum, London, UK; [c]European Space Research and Technology Centre (ESA/ESTEC), Directorate of Human and Robotic Exploration, Noordwijk, Netherlands; [d]European Space Research and Technology Centre (ESA/ESTEC), Directorate of Science, Noordwijk, Netherlands; [e]German Aerospace Center (DLR), Institute of Planetary Research Rutherfordstr, Berlin, Germany; [f]Istituto Nazionale di Astrofisica Osservatorio Astronomico di Padova Vicolo dell'Osservatorio, Padova, Italy; [g]Istituto di Astrofisica e Planetologia Spaziali, Istituto Nazionale di Astrofisica, Rome, Italy; [h]Laboratoire de Planétologie et Géodynamique, LPG Nantes, Nantes, France; [i]Université Paris Saclay – CNRS – Institute d'Astrophysique Spatiale, Orsay, France; [j]Space Research Centre, University of Leicester, Leicester, UK; [k]Univ Lyon, Univ Lyon 1, ENSL, CNRS, LGL-TPE, Villeurbanne, France; [l]Physikalisches Institut, University of Bern, Bern, Switzerland

**ABSTRACT**

We present the geography of Oxia Planum, the landing site for the ExoMars 2022 mission. This map provides the planetary science community with a framework to understand this, until recently, unexplored area. The map comprises (1) a mosaic of the panchromatic Context Camera (CTX) Digital Elevation Models (DEM) and Ortho Rectified Images (ORI) controlled to the High Resolution Stereo Camera (HRSC) multiorbit Digital Elevation Models (DEM) and (2) a mosaic of Colour and Stereo Surface Imaging System (CaSSIS) synthetic colour data products, registered to the CTX ORI mosaic. We define a grid of exploration quadrangles (quads) and an informal group of geographic regions to describe Oxia Planum. These regions bridge the scale gap between features observed on large areas (~100s km$^2$) and the local geography (10s km$^2$) relevant to the Rosalind Franklin rover's operations in Oxia Planum.

**ARTICLE HISTORY**
Received 20 May 2021
Revised 3 September 2021
Accepted 6 September 2021

**KEYWORDS**
ExoMars; Oxia Planum; Mars; CaSSIS; CTX DEM; geography

## Highlights

- The Geography and a CaSSIS mosaic of Oxia Planum, the ExoMars rover landing site.

## 1. Introduction

ExoMars 2022 is a cooperative mission between the European Space Agency (ESA) and Roscosmos, the Russian space organisation consisting of the ExoMars rover 'Rosalind Franklin' and the instrumented lander 'Kazakoch'. The mission is tasked with searching for signs of past and present life on Mars (Figure 1) and will investigate the geochemical environment in the shallow subsurface over a nominal mission of 218 Martian days (sols; Vago et al., 2017) in Oxia Planum. The rover's search for signs of life is predicated on identifying the best possible locations for assessing three parameters (1) geological context consistent with life-hospitable conditions, (2) potential chemical biosignatures, and (3) possible physical biosignatures. To select those locations a good understanding of the landing site's geology based on the available orbital information is required.

Oxia Planum is situated on the northern margin of Arabia Terra (Figure 1) and preserves a record of the diverse geological processes that have shaped the region. It is in a transitional region between the heavily cratered Noachian-aged Arabia Terra (>3.7 Ga; Hartmann & Neukum, 2001, Tanaka et al., 2014a, 2014b) and the younger low-lying Hesperian/Amazonian-aged plains of Chryse Planitia (<3.0 Ga; Hartmann & Neukum, 2001). This area has been selected as the landing site because of its abundance of Noachian-aged material, including regional phyllosilicate-bearing deposits (Figure 2; Carter et al., 2015; Noe Dobrea et al., 2010), which are evidence for widespread aqueous alteration (Mandon et al., 2021; Quantin-Nataf et al., 2021), and occur at a sufficiently low elevation to permit landing (Vago et al., 2018). Oxia Planum records the Noachian basement formation (Pan et al., 2019) and the formation of global-scale tectonic fabrics (Anderson et al., 2001). The region was extensively modified in the late Noachian/Hesperian period, as shown by evidence of fluvial and paleo-lake activity (Fawdon et al., 2019;

CONTACT Peter Fawdon peter.fawdon@open.ac.uk School of Physical Sciences, Open University, Milton Keynes, Buckinghamshire MK7 6AA, UK
Supplemental data for this article can be accessed at https://doi.org/10.1080/17445647.2021.1982035

© 2021 The Author(s). Published by Informa UK Limited, trading as Taylor & Francis Group.
This is an Open Access article distributed under the terms of the Creative Commons Attribution License (http://creativecommons.org/licenses/by/4.0/), which permits unrestricted use, distribution, and reproduction in any medium, provided the original work is properly cited.

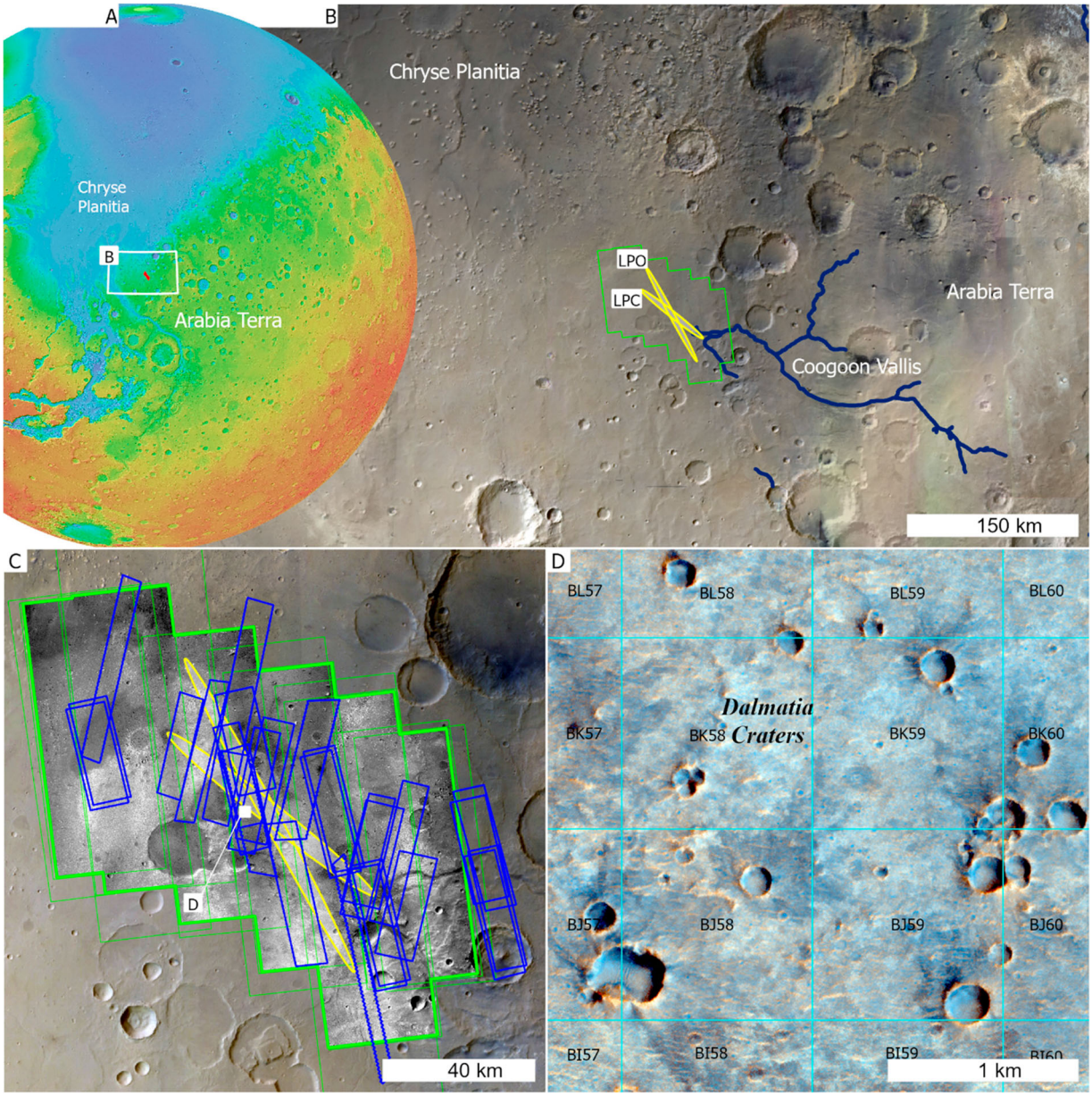



**Figure 1.** Location of Oxia Planum and illustration of the ExoMars rover The landing site for the ExoMars mission in (A) Oxia Planum on the northern margin of Arabia Terra shown here in MOLA topography (Smith et al., 2001). (B) Rosalind Franklin and the Kazakoch platform are scheduled to land in the 100 km landing ellipse in early 2023. Yellow ellipses (in B and C) denote the opening (LPO) and closing (LPC) of the scheduled 2022 launch possibilities seen here with the outline of the CTX DEM mosaic overlain on the HRSC Colour mosaic of the MC11 Oxia Plaus quadrangle. (C) Coverage of the data sets presented on the main map. Green = CTX footprints, Blue = CaSSIS footprints overlain on HRSC base map tile MC11W24_co5ps. (D) Example of the 1 × 1 km 'quads' and quad naming over CaSSIS synthetic RGB image MY35_008275_165_0 close to the centre of the landing ellipses.

Gary-Bicas & Rogers, 2021; Mandon et al., 2021; Molina et al., 2017; Cathy Quantin-Nataf et al., 2021), possible shoreline formation (Dickeson & Davis, 2020), volcanism (Michalski & Bleacher, 2013), and alteration to form phyllosilicate deposits (Carter et al., 2015). The surface continues to be modified by aeolian transport and erosion processes (Favaro et al., 2021; Silvestro et al., 2021) and by impact cratering (Fawdon et al., 2020).

The first step in the process of identifying the best possible sample locations requires assembling the relevant data and establishing a framework of conventions to describe them. The 'Macro' sub-group of the Rover Science Operations Working Group (RSOWG) was created to characterise the landing site to a fidelity relevant for rover operations; that is, at metre-scale. The rover is capable of driving approximately 30–100 m per day, depending on the terrain's complexity. The RSOWG 'Macro- sub-group is studying the landing site (an area on the order of ~1000 km$^2$) to consider the geological processes that might affect the potential for formation, concentration, and preservation of biomarkers in the 'one-sigma' landing ellipse (i.e. the ~66.75 × 5 km uncertainty ellipse with ~67% touchdown probability; Figure 1). The 'Macro' sub-group organised a high-

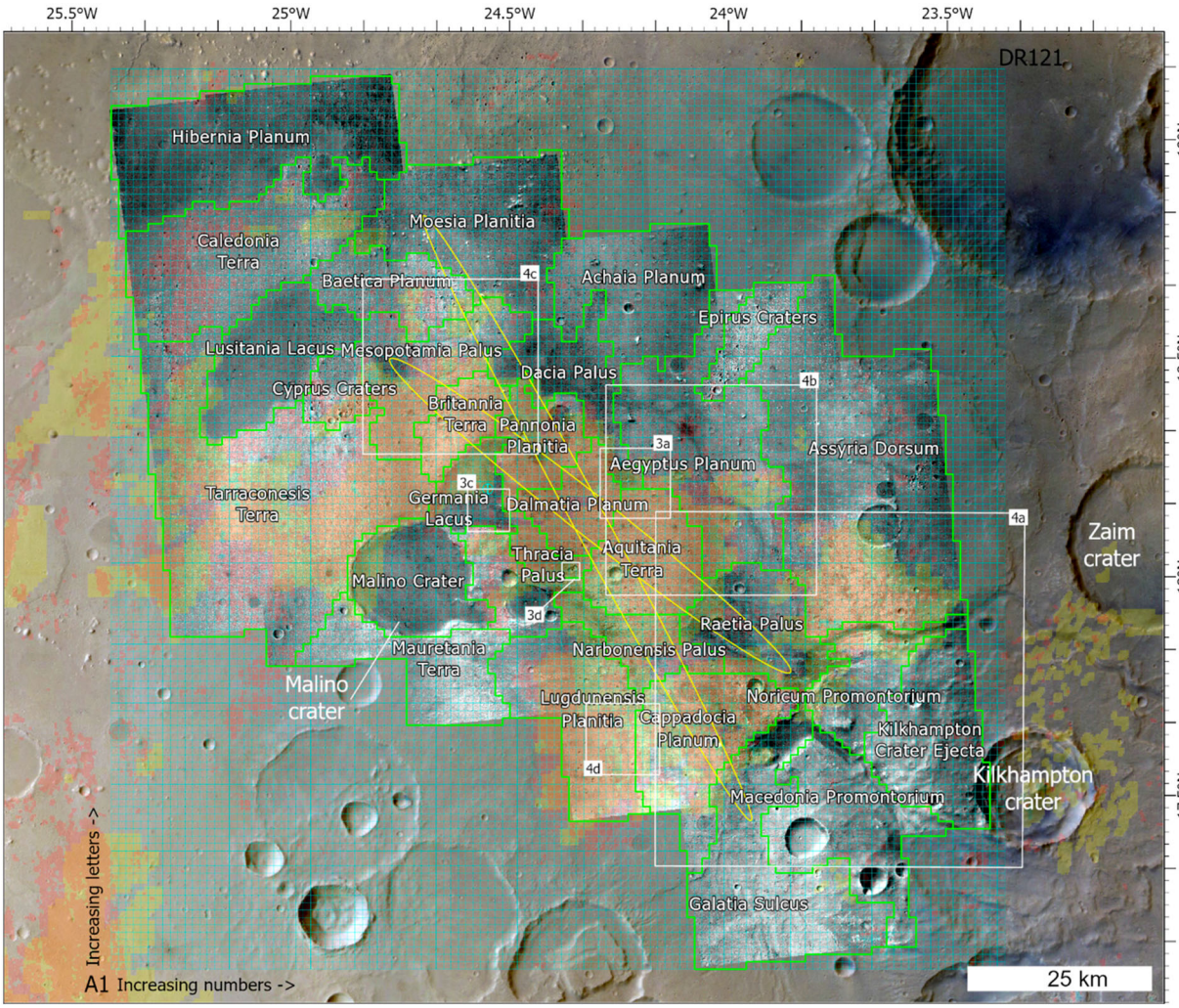



**Figure 2.** Map to geographic regions. The operations grid of 1 × 1 km quads (cyan) and geographic regions (green; Table 3) created for ExoMars 2022 rover operations. Quad labeling starts with row 'A' column '1' in the South West progressing to row 'DR' and column '121' in the North East with the central longitude of the projection (section 2.1) located in Germania Lacus (cyan cross). Landing ellipses for the opening (high azimuth) and close (low azimuth) of the launch window (yellow) overlain on the CTX ORI mosaic with a map of phyllosilicate detections from CRISM (red shading) and OMEGA (yellow shading) observations (Quantin-Nataf et al., 2021) over the HRSC pan-sharpened colour mosaic base layer.

resolution geologic mapping campaign between May 2019 and August 2020 (Sefton-Nash et al., 2020). The principal objectives of this exercise were to (i) familiarise scientists with the geography and geology of the landing site and (ii) create a geological map to build and guide the mission's strategic plan, making the best uses of the available resources (e.g. time, power, data) to find locations for sample acquisition and analysis.

As part of this process, several base map data products were created to build a geographic framework in the region around Oxia Planum. We present a map and data package of Oxia Planum to enable the planetary science community to explore the landing site. This includes

(1). A grid of exploration quadrangles (quads) and an informal group of regions to describe the geography of Oxia Planum (Figure 2). These bridge the descriptive scale gap between features named by the International Astronomical Union (IAU) (~100s km$^2$) and the local landscape (10s km$^2$) relevant to *Rosalind Franklin* operations.

(2). Mosaics of the Context Camera (CTX; Malin et al., 2007) Digital Elevation Models (DEM) at 20 m/pixel and Orthorectified Images (ORI) at 6 m/pixel (Figure 1). These data are projected onto a High Resolution Stereo Camera (HRSC; Neukum et al., 2004) multi-orbit DEM (50 m cell size) and corresponding 12.5 m/pixel panchromatic mosaic (Gwinner et al., 2016), which in turn is fixed to the Mars Orbiter Laser Altimeter (MOLA; Smith et al., 2001) geodetic control network. The CTX mosaic provides a base layer for registration of other higher resolution data sets (e.g. Volat & Quantan-Nataf, 2020).

(3). The Colour and Stereo Surface Imaging System (CaSSIS; Thomas et al., 2017) colour data products at 4 m/pixel acquired for Oxia Planum and registered to the CTX ORI mosaic. Data

collection for CaSSIS is ongoing and we will update this database as new observations are obtained.

## 2. Data and methods

### 2.1. Data

#### 2.1.1. High Resolution Stereo Camera (HRSC)

The Mars Express High Resolution Stereo Camera (HRSC; Gwinner et al., 2016) MC11 multi-orbit DEM (Kersten et al., 2018) is used as the base control map. It is controlled to the global Mars Orbiter Laser Altimeter (MOLA; Smith et al., 2001) DEM (~463 m cell size), currently the most accurate global geodetic dataset for Mars.

#### 2.1.2. Context Camera (CTX) and CTX Digital Elevation Models (DEM)

The CTX camera onboard the Mars Reconnaissance Orbiter provides ~6 m/pixel panchromatic data with a swath width of ~20 km (Malin et al., 2007). The main map is a mosaic of six ORI and DEM created from CTX images for which the emission angles and coverage allowed stereo pairs to be used for photogrammetric reconstruction and DEM production (Figure 1, Table 1).

Our CTX DEMs were created following the method of Kirk et al. (2008), using public-domain Integrated Software for Images and Spectrometers (ISIS3) software to pre-process the raw Experimental Data Records (EDR). The EDRs were then processed in SocetSet®, a commercially available photogrammetry suite (http://www.socetset.com), with X, Y, and Z co-ordinates of the DEM controlled to MOLA Point Experimental Data Record (PEDR) data. The ORI and DEM were then post-processed in ISIS, mosaicked in the software Environment for Visualising Images (ENVI), before manual georeferencing in ArcGIS software. Finally, the georeferenced image mosaic was blended in Adobe Photoshop to remove seamlines using the Avenza Geographic Imager extension to retain geospatial information in the blended product.

The output from SocetSet® are 20 m/pixel DEM (resolving topography of ~50–60 m features) and 12 orthorectified CTX images with a scale of 6 m/pixel. The Expected Vertical Precision (EVP) in each CTX DEM can be estimated based on viewing geometry and pixel scale (Kirk et al., 2003, 2008), e.g. EVP = Δ p IFOV / (parallax/height) where **Δ p** is the Root Mean Square (RMS) stereo matching error in pixel units, assumed to be 0.2 pixels (Cook et al., 1996) and confirmed with matching software for several other planetary image data sets (Howington-Kraus et al., 2002; Kirk et al., 1999). The pixel matching error is influenced by signal-to-noise ratio, scene contrast and differences in illumination between the images. Pattern noise can also be introduced by the automatic terrain extraction algorithm, especially in areas of low correlation. These can be identified as patches of 'triangles' in the hill shade model (e.g. smooth, low contrast slopes and along shadows). **IFOV** is the instantaneous field of view of the image on the ground (pixel size in metres). If the paired images have different IFOVs, the RMS value is used, e.g. IFOV = $\sqrt{}$(pixel scale image 1 + pixel scale image 2). The **parallax/height** ratio, calculated from the three-dimensional intersection geometry, reduces to tan(e) for an image with emission angle 'e' paired with a nadir image, e.g. parallax/height = tan(e), where e = |emission angle 1 − emission angle 2|.

#### 2.1.3. Colour and Stereo Surface Imaging System (CaSSIS)

The Colour and Stereo Surface Imaging System (CaSSIS; Thomas et al., 2017) instrument on the ESA Trace Gas Orbiter (TGO) continues to observe the ExoMars landing site (Figure 1). CaSSIS collects data with four filters (Infrared (IR); 950 nm, Near-Infrared (NIR); 850 nm, broad transmission, Panchromatic, filter (PAN); 650 nm and BLUE–GREEN; 475 nm), chosen to provide the camera with a limited multispectral capability sensitive to a variety of minerals (Tornabene et al., 2017). CaSSIS has a swath width of ~9 km and a rotation mechanism to permit stereo acquisitions. We use CaSSIS 3 or 4 band cubes for our scientific investigation of Oxia Planum. A mosaic of synthetic RGB

**Table 1** . CTX images. CTX images used in the DTM mosaic and their Expected Vertical Precision (EVP) sorted by longitude.

| CTX image pairs (E-W) | Centre (Lat, Long) | Emission angle (°) | Pixel size (m) | EVP (m) |
|---|---|---|---|---|
| J14_050138_1986_XN_18N025W | 18.66°N 334.94°E | 28.34 | 7.14 | **DEM 1** |
| K05_055518_1986_XN_18N025W | 18.69°N 334.89°E | 5.69 | 5.64 | 1.71 |
| F21_044178_1988_XN_18N024W | 18.83°N 335.12°E | 28.08 | 7.08 | **DEM 2** |
| J05_046723_1985_XN_18N025W | 18.57°N 335.08°E | 0.09 | 5.59 | 1.34 |
| F03_037136_1977_XN_17N023W | 17.81°N 336.10°E | 14.95 | 5.95 | **DEM 3** |
| F23_044956_1984_XN_18N024W | 18.49°N 335.44°E | 3.35 | 5.59 | 3.31 |
| J01_045167_1983_XN_18N024W | 18.33°N 335.80°E | 1.48 | 5.56 | **DEM 4** |
| J03_045800_1983_XN_18N024W | 18.33°N 335.75°E | 14.05 | 5.93 | 3.04 |
| F03_037070_1980_XN_18N024W | 18.09°N 336.09°E | 8.63 | 5.70 | **DEM 5** |
| F03_037136_1977_XN_17N023W | 17.81°N 336.10°E | 14.95 | 5.95 | 6.16 |
| J01_045101_1981_XN_18N023W | 18.16°N 336.29°E | 11.59 | 5.78 | **DEM 6** |
| J02_045378_1981_XN_18N023W | 18.14°N 336.37°E | 0.85 | 5.57 | 3.55 |

**Table 2.** CaSSIS observations. CaSSIS observations over Oxia Planum as of 01/01/2021.

| Image ID | Filters | Incidence angle (°) | Local time | Solar longitude ($L_s$) | Synthetic RGB in mosaic | Georeferenced ISIS cube in data repository |
|---|---|---|---|---|---|---|
| MY34_001934_162_0 | PAN-RED-NIR-BLU | 48.151 | 08:50:20 | 167.71 | Yes | |
| MY34_002021_162_0 | PAN-RED-NIR | 71.402 | 07:13:42 | 171.60 | Yes | |
| MY34_003806_019_1 | PAN-RED-BLU | 53.130 | 09:51:29 | 260.06 | | |
| MY34_003806_019_2 | PAN-NIR-BLU | 53.027 | 09:52:13 | 260.06 | Yes | Yes |
| MY34_003893_018_1 | PAN-NIR-BLU | 71.037 | 08:07:36 | 264.56 | | |
| MY34_003893_018_2 | PAN-RED-BLU | 70.803 | 08:07:55 | 264.56 | Yes | |
| MY34_004085_162_1 | PAN-RED-BLU | 68.856 | 15:37:41 | 274.47 | Yes | |
| MY34_004085_162_2 | PAN-NIR-BLU | 69.017 | 15:38:32 | 274.47 | Yes | |
| MY34_004172_162_1 | PAN-NIR-BLU | 51.901 | 13:54:02 | 278.91 | Yes | |
| MY34_004172_162_2 | PAN-RED-BLU | 52.007 | 13:54:51 | 278.91 | | |
| MY34_004259_162_1 | PAN | 43.119 | 12:12:25 | 283.33 | | |
| MY34_004259_162_2 | PAN-NIR-BLU | 43.127 | 12:13:11 | 283.33 | Yes | |
| MY34_004925_019_2 | PAN-NIR-BLU | 35.367 | 12:07:21 | 315.88 | Yes | |
| MY34_005012_018_1 | PAN-BLU | 40.932 | 10:25:46 | 319.95 | Yes | |
| MY34_005012_018_2 | PAN-NIR-BLU | 40.814 | 10:26:26 | 319.95 | Yes | |
| MY34_005378_162_1 | PAN-RED-BLU | 50.339 | 14:48:19 | 336.53 | Yes | |
| MY34_005378_162_2 | PAN-NIR-BLU | 50.513 | 14:49:10 | 336.53 | Yes | |
| MY34_005664_163_1 | PAN-RED-BLU | 42.428 | 09:35:09 | 348.90 | Yes | |
| MY34_005664_163_2 | PAN-NIR-BLU | 42.251 | 09:36:00 | 348.90 | Yes | |
| MY35_006504_018_0 | PAN-NIR-BLU | 74.907 | 06:51:39 | 22.62 | Yes | Yes |
| MY35_007250_019_0 | PAN-RED-NIR-BLU | 77.254 | 17:29:53 | 50.29 | | |
| MY35_007337_020_0 | PAN-RED-NIR-BLU | 56.277 | 15:59:01 | 53.44 | Yes | |
| MY35_007536_021_0 | PAN-RED-NIR-BLU | 8.678 | 12:34:18 | 60.59 | Yes | |
| MY35_007623_019_0 | PAN-RED-NIR-BLU | 14.604 | 11:00:19 | 63.71 | Yes | |
| MY35_008275_165_0 | PAN-NIR-BLU | 16.007 | 10:56:45 | 87.07 | Yes | Yes |
| MY35_008742_019_0 | PAN-RED-NIR-BLU | 47.860 | 15:24:50 | 104.06 | Yes | Yes |
| MY35_009394_165_0 | PAN-NIR-BLU | 46.484 | 15:17:22 | 128.83 | | |
| MY35_009481_165_0 | PAN-NIR-BLU | 24.363 | 13:42:46 | 132.27 | Yes | Yes |
| MY35_012092_163_0 | PAN-RED-NIR-BLU | 60.915 | 14:58:52 | 254.60 | Yes | |
| MY35_013584_163_0 | PAN-NIR-BLU | 32.105 | 11:33:20 | 328.27 | Yes | Yes |
| MY35_013584_163_0 | PAN-NIR-BLU | 32.099 | 11:33:26 | 328.27 | | |
| MY35_013964_017_0 | PAN-NIR-BLU | 85.415 | 17:32:13 | 345.01 | | |
| MY36_014424_021_0 | PAN-RED-NIR-BLU | 39.31 | 09:33:25 | 4.15 | | |
| MY36_014616_153_0 | PAN-NIR-BLU | 82.147 | 17:33:43 | 11.82 | | |
| MY36_014989_162_0 | PAN-RED-NIR-BLU | 15.312 | 11:04:00 | 26.24 | | |
| MY36_015275_161_0 | PAN-NIR-BLU | 82.588 | 06:11:41 | 36.95 | | |
| MY36_015369_018_0 | PAN-RED-NIR-BLU | 74.601 | 17:15:38 | 40.4 | | |
| MY36_015456_017_0 | PAN-RED-NIR-BLU | 52.586 | 15:41:18 | 43.59 | | |

products is presented on the main map. Synthetic RGB products use a combination of PAN and BLUE filter images whereby: The Red channel is the PAN filter mosaic, The Green channel is a combination of a low pass filter of the Blue and a high pass filter of the PAN, incorporating colour information from BLUE and spatial information of PAN. The Blue channel is a combination of PAN and BLUE–GREEN such that each pixel has a value of (2*BLU – 0.3*PAN). Each channel is individually contrast-enhanced to form the final product. As TGO operates in a non-sun synchronous orbit, surface overflights repeat every 36 days spanning a range of local times and seasons (Table 2), individual images do not necessarily have appropriate viewing angles, lighting and atmospheric conditions conducive to the creation of a consistent mosaic data set. We will continue to update the database of georeferenced images as more appropriate images are collected by TGO (see Section 6).

## 2.2. Making the map

### 2.2.1. Projection

The map is presented in an equirectangular projection centred at, 335.45°E, (24.55°W) based on the IAU Mars2000 sphere. This matches the coordinate system used by the ExoMars Rover Operations Control Centre (ROCC) to minimise local distortion. This is important for maintaining accuracy between remote sensing observation and rover scale operations. And is available with the supporting data sets (Table 4).

### 2.2.2 Georeferencing and registration

Registration of the CTX DEM mosaic to the HRSC dataset used ~200 manual tie points between the CTX ORI and HRSC image mosaic and these tie points were then applied to the DEM mosaic. Georeferencing and registration of the CaSSIS data used an initial set of manual tie points to seed the automatic generation of additional tie points using ArcPro 2.7 software. The CTX mosaic and CaSSIS data were rectified using the spline transformation, which optimises for local but not global accuracy (Esri, 2020). This method provided good results for images with a range of viewing angles and accounts well for local adjustments needed for abrupt elevation changes.

### 2.2.3. Quad grid and contours

The quad grid was created using the ArcPro 2.7 Grid Index Features Tool (Esri, 2021). The grid is a 121 ×

120 array of 1000 m × 1000 m quads labelled 'A1' in the South West to 'DP120' in the North East. The grid covers the entire CTX mosaic and the lower left corner of quad BD50 coincides with the centre of the ROCC projection system at 335.45°E 18.20°N. Topographic contours were created at 25 m intervals from a CTX DEM downsampled to 100 m/pixel, with contours shorter than 1500 m in length were removed. Contours were smoothed using the PAEK algorithm at a tolerance of 200 m (USGS & MRCTR GIS Lab, 2018).

### 2.3. Geographic regions

A common geographical division and naming system for the Oxia Planum region is needed to allow ExoMars team members to communicate efficiently. Identifying and naming geographical locations and zones provides a spatial context for detailed observations, strategic planning and operations, and hypotheses testing.

#### 2.3.1. Differentiating geographic regions

We divide Oxia Planum into 30 regions (Figure 2 and Table 3). This system of regions is a formalisation of the geographic differentiation demanded by discussions since the initial suggestion of Oxia Planum as a landing site in 2014 (ESA & The ExoMars 2018 Landing Site Selection Working Group (LSSWG), 2014) Each region is defined by a combination of topographic and or albedo changes in the HRSC and CTX data and that have needed to be talked about. Regions are smaller closer to the centre of the landing site or where topography and albedo are more variable. This reflects the need to increase the fidelity of discussion where the rover is more likely to land or there are likely to have been more active geomorphic processes. As such these regions capture features pertaining to hypotheses about the paleo-environments being developed by the RSOWG and provide a natural framework to explore Oxia Planum.

#### 2.3.2. Naming geographic regions

The regions were named in three ways: a number, a unique identifier, and a descriptive term. Unique identifiers were drawn from a list of Roman imperial and senatorial provinces at the largest geographic extent of the Roman empire in 117AD. This scheme was chosen because it has geographic and cultural ties throughout Europe and provides an appropriate number and variety of names. The descriptive terms (e.g. *Planum*, *Lacus*, etc) are those used in planetary toponomy (IAU, 1979). Names were selected to reflect the geography of the region (e.g. Caledonia has high elevation terrain in the northwest, Aegyptus has a large channel feature). Geographic locations within regions are also named. These names were drawn from a wider list of Roman towns or other relevant geographic locations with suitable, but process-agnostic, descriptive term (e.g. Alexandria Tholus named after the city in the 'Aegyptus' imperial province). These conventions have the capacity to expand this list as an exploration of Oxia Planum continues.

Although IAU recognised features (e.g. Malino crater) have also been included, all other names are informal. Informal naming of local features has been performed by previous Mars Rover mission teams. As has occurred during previous missions, some names will probably be replaced with formal IAU designations as the mission progresses.

## 3. Results, observations and preliminary interpretations

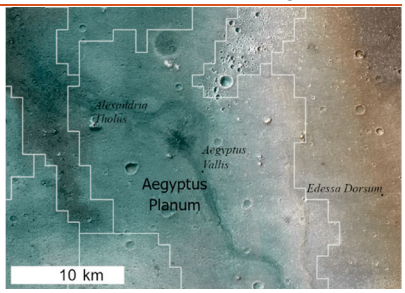
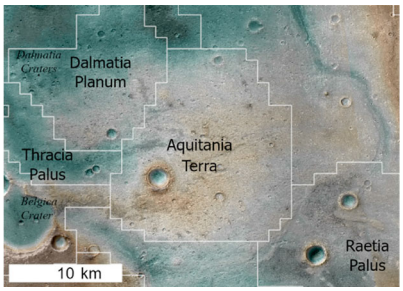
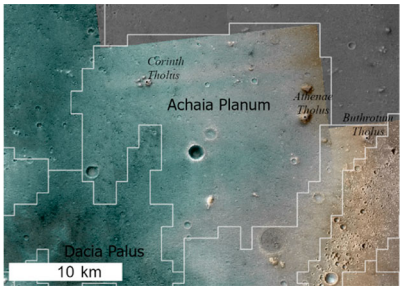
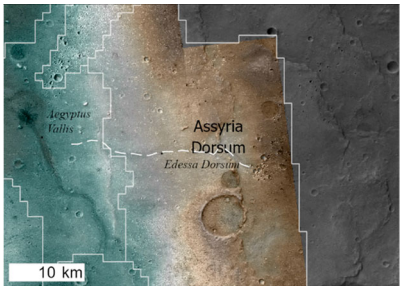
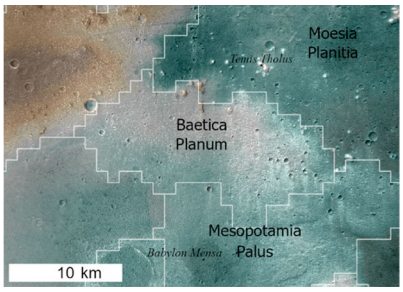
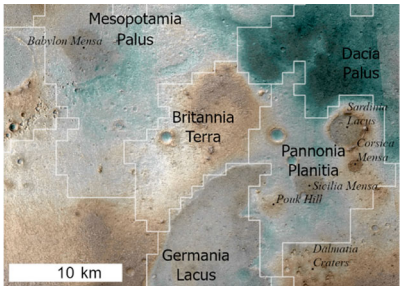
### 3.1. Geographic regions

The main map (CTX DEM and ORI mosaics) covers 8750 $km^2$ and elevations ranging from −2404 m in the South East to −3240 m to the North. The geographic regions and geographic location we identified in Oxia Planum are shown in Figure 2, with further description in Table 3.

### 3.2. Surface colours

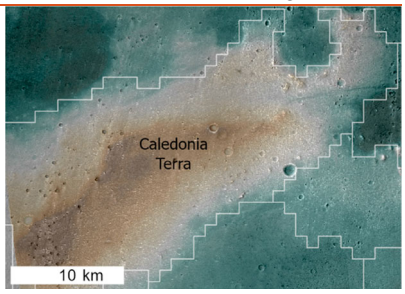
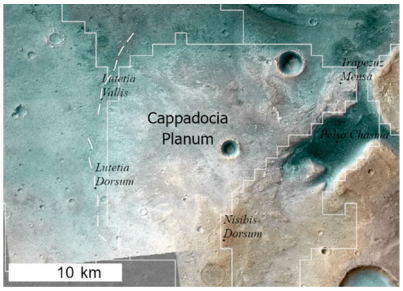
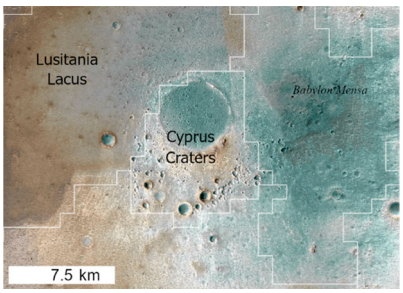
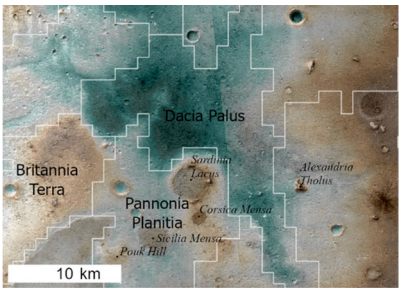
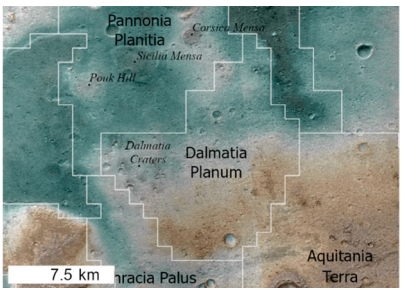
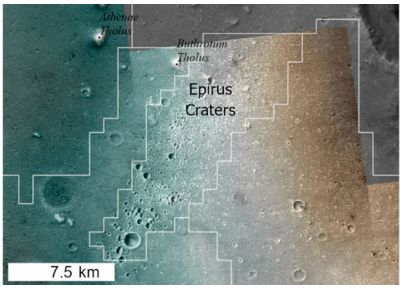
CTX and CaSSIS data provide relative albedo and colour information about Oxia Planum. Light-toned terrains in CTX data often have a 'white' or 'orangey' colour in CaSSIS images and are associated with higher elevation terrains in the South, East, and West of the map. These areas correlate with observations of phyllosilicate minerals (Figure 2) and possible sub-horizontal layering and widespread metre scale fracturing in the bedrock. Details of these relationships are explored in Parkes Bowen et al. (2021). In the northern and central regions, the dark surface materials onlap the bright clay-bearing terrains and embay a widespread population of bright buttes (McNeil et al., 2021) but darker areas with diffuse margins also occur in other topographic lows (e.g. central *Dalmatia*). Many of these surfaces are covered by aeolian bedforms (Favaro et al., 2021; Silvestro et al., 2021; Figure 3), dominated by mafic mineralogy (Gary-Bicas & Rogers, 2021; Cathy Quantin-Nataf et al., 2021). Darker toned and 'blueish' surfaces occur in low elevation regions (e.g. *Germania*), but are also seen capping mesas (e.g. *Corsica*). The mesa caprocks shed boulders at their marginal scarps, suggesting a consolidated material. However, toward the centre of these regions the colours change to be relatively light toned and 'orangey' (Figure 3) suggesting that this resistant dark-toned relatively bluish material is only a thin layer.

**Table 3.** The geographic regions of Oxia Planum. Characteristics of each geographic region in Oxia Planum shown in CTX mosaic overlain by the colour shaded DEM mosaic with lower elevations (teal) towards higher elevation areas (brown).

| Region *Type* | Description<br>Additional information | Appearance and topography<br>(Teal = low, Brown = high) |
|---|---|---|
| 01<br>**Aegyptus**<br>*Planum* | Gently sloping plain crossed by a 500 m wide channel, *Aegyptus Vallis*.<br>*Alexandria Tholus* is one of several isolated buttes in the region. The western margin is marked by an N-S subtle ridge. A fresh impact crater is marked by a dark rayed ejecta. |  |
| 02<br>**Aquitania**<br>*Terra* | Topographic high region in the centre of Oxia Planum, surface characterised by bright E-W trending, ten-metre-scale wide, ridges.<br>These light-toned/orange tinged surfaces have spectral signatures indicating the presence of hydrated phyllosilicate minerals |  |
| 03<br>**Archaia**<br>*Planum* | Smooth plain in the northeast of the study area; contains numerous light-toned buttes |  |
| 04<br>**Assyria**<br>*Dorsum* | High elevation terrain forming a N-S trending asymmetrical ridge. The south and east are light toned, while the lower elevation areas in the northwest are darker in tone. The region is crosscut W-E *by Edessa Dorsum,* a narrow ridge that sits in a local topographic low. |  |
| 05<br>**Baetica**<br>*Planum* | Relatively high elevation region of light-toned terrain bounded to the north by dark plains.<br>In this region, rounded buttes directly overlie clay-bearing terrains. |  |
| 06<br>**Britannia**<br>*Terra* | High elevation bright terrain with numerous rough irregular knobs; well defined boundary at the south with Germania Lacus. |  |

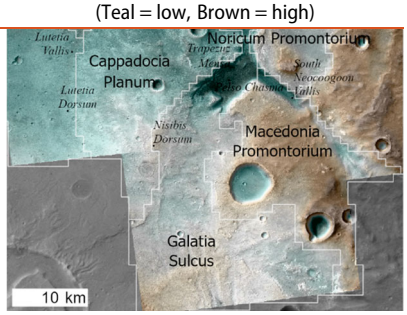
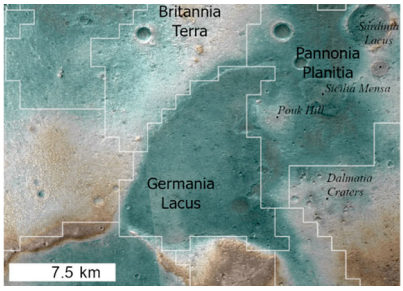
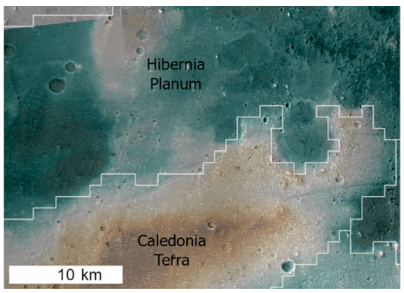
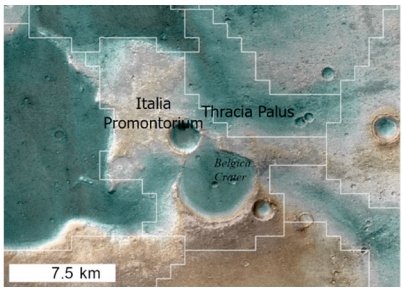
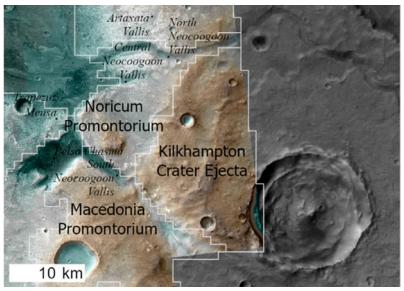
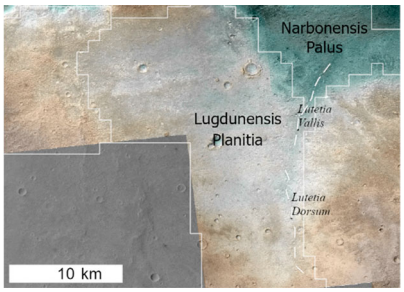
(*Continued*)

**Table 3.** Continued.

| Region *Type* | Description<br>Additional information | Appearance and topography<br>(Teal = low, Brown = high) |
|---|---|---|
| 07<br>**Caledonia**<br>*Terra* | High elevation terrain in the far north of the region, forming an arcuate ridge ~150 m high and 10–20 km across. |  |
| 08<br>**Cappadocia**<br>*Planum* | Plain sloping to the NE formed of a mix of dark and light toned terrains with a promontory in the west of bright layered materials. |  |
| 09<br>**Cyprus**<br>*Craters* | Cluster of fresh impact craters and high-standing terrain associated with an infilled and degraded crater rim. |  |
| 10<br>**Dacia**<br>*Palus* | Low-lying dark-toned terrain with a sinuous southern margin at ~ −3125 m elevation. |  |
| 11<br>**Dalmatia**<br>*Planum* | Intermediate relief terrain with mottled tones that appears to be transitional between Aquitania Terra and Pannonia Planitia.<br>A small cluster of impact craters with distinct dark ejecta occurs in the west of the zone. |  |
| 12<br>**Epirus**<br>*Craters* | An elongate cluster of small fresh impact craters in the northeast of the region; probably a chain of secondary impact craters originating from a much larger impact far to the southwest. |  |

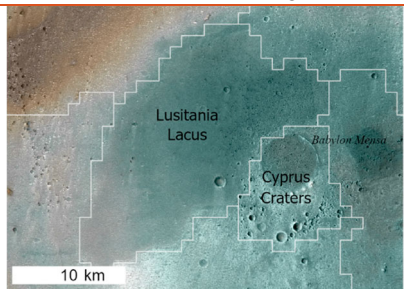
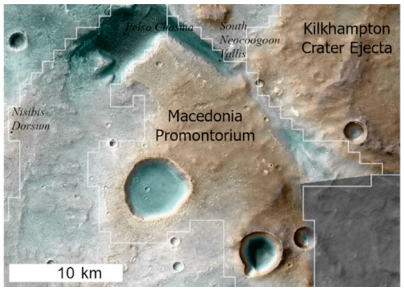
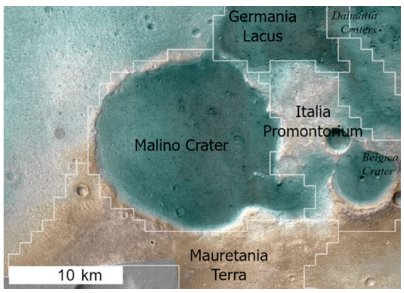
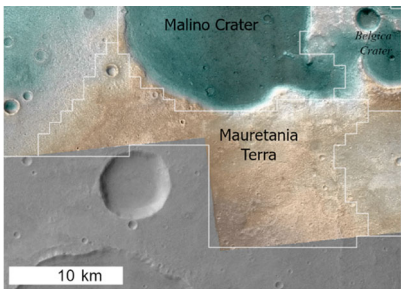
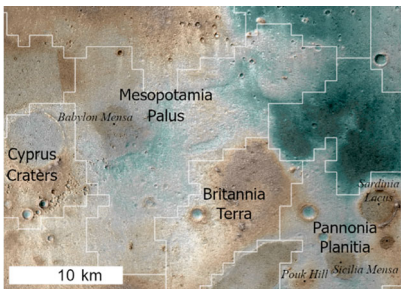
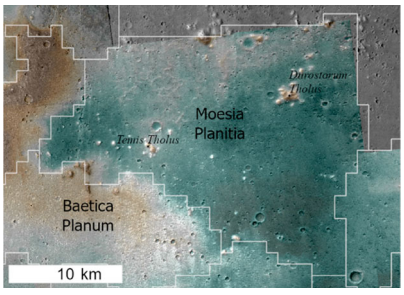
(*Continued*)

**Table 3.** Continued.

| Region *Type* | Description<br>Additional information | Appearance and topography<br>(Teal = low, Brown = high) |
|---|---|---|
| 13<br>**Galatia**<br>*Sulcus* | A series of linear channels incised into light-toned layered terrains.<br>The channels end in Polus Chasma, a The northwest is bounded by a tectonic ridge and a channel southeast excavates a light toned layer. |  |
| 14<br>**Germania**<br>*Lacus* | A low elevation zone of low relief, dark toned plains. Darker toned material dominates towards the edges and the centre has a brighter albedo, bounded to the west by higher elevation terrain and to the east by a subtle moat. Eastern bounding scarp of light toned material with a thin dark top. |  |
| 15<br>**Hibernia**<br>*Planum* | Low elevation terrain in the far north west of the landing site. This region is bisected by a wide, N-S trending ridge. The topography also shows several quasi-circular depressions that are probably ancient impact structures. |  |
| 16<br>**Italia**<br>*Promontorium* | High elevation terrain in the south west. The western part of the region forms the rim of Malino crater.<br>A narrow band of upstanding, terrain connects to Aquitania Terra to the northwest. The rim of Belgica crater is breached in two places, creating a connection between sediment fans to the east of Milano crater. |  |
| 17<br>**Kilkhampton crater**<br>*(IAU feature no. 15849)* | Double-layered impact ejecta associated with Kilkhampton crater which lies just outside the map area.<br>Impact ejecta overlies *North* and *South Neocoogoon Vallis* in *Noricum Promontorium* |  |
| 18<br>**Lugdunensis**<br>*Planitia* | Light toned plain in the south of the landing site area that slopes gently to the northeast. A shallow valley in the east (*Lutetia Vallis)* trends to the north and defines the boundary with Cappadocia to the east. Lugdunensis contains many inverted terrain features, including ridge (*Lutetia Dorsum*) that runs along the axis of the topographic low containing Lutetia Vallis. |  |

(*Continued*)

**Table 3.** Continued.

| Region *Type* | Description<br>Additional information | Appearance and topography<br>(Teal = low, Brown = high) |
|---|---|---|
| 19<br>**Lusitania**<br>*Lacus* | Low relief, low elevation plain in the east of the region. The dark surface retains numerous small craters and is brighter at its margins. A scarp of light-toned material, and an external 'moat' define the boundary of the dark-toned plains. |  |
| 20<br>**Macedonia**<br>*Promontorium* | High elevation terrain in the southeast of the region. Light toned layered terrains are overlain by impact ejecta from Kilkhampton crater. The northern boundary is the *South Neocoogoon Vallis,* a ~140 m deep and ~1400 m wide 'U'-shaped valley, that is itself incised into a wider valley – as demonstrated by a terrace along the northern edge of *Macedonia Promontorium.* |  |
| 21<br>**Malino**<br>*Crater*<br>*(IAU feature no. 15892)* | Malino is a 15 km diameter, degraded impact crater. The floor of the crater is covered by low relief, dark-toned materials that onlap light-toned terrains at breaches in the crater rims to the north and east. |  |
| 22<br>**Mauretania**<br>*Terra* | High elevation, rough, light toned terrain immediately south of the Malino Crater region. |  |
| 23 **Mesopotamia**<br>*Palus* | Low elevation, light-toned terrain that slopes inwards and to the northeast towards the low-lying region of *Dacia Palus,* forming a shallow valley. |  |
| 24<br>**Moesia**<br>*Planitia* | Low elevation terrain in the north of the study area. The dark material of the region has sharp contacts with bright surfaces to the south west. Several clusters of bright mounds straddle this margin and are embayed by the dark terrain. |  |

(*Continued*)

**Table 3.** Continued.

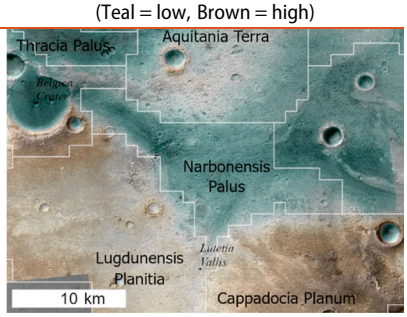
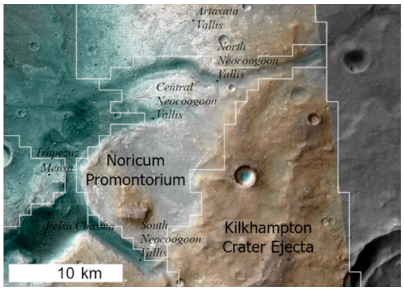
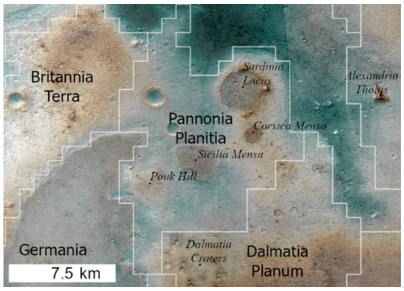
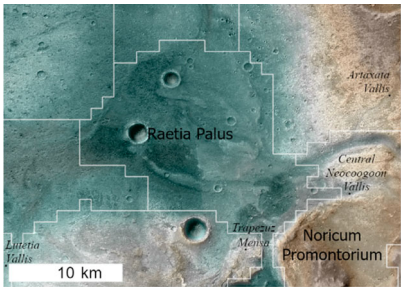
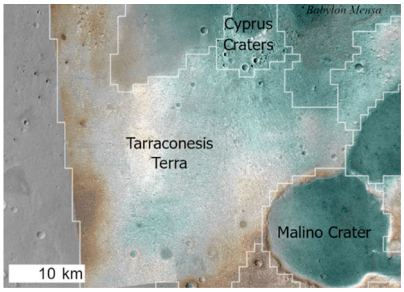
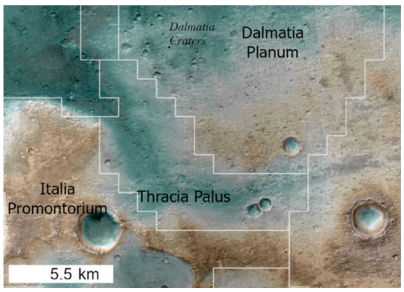
| Region *Type* | Description<br>Additional information | Appearance and topography<br>(Teal = low, Brown = high) |
|---|---|---|
| 25<br>**Narbonensis**<br>*Palus* | Low elevation region topographically connected to the sediment fans in *Raetia Palus*. Also connected to *Lutetia Vallis* in *Lugdunensis* Planitia to the south. |  |
| 26<br>**Noricum**<br>*Promontorium* | Light-toned, layered promontory with patches of superposing dark material. The promontory is incised by *North Neocoogoon Vallis* and *central Neocoogoon Vallis* channels. |  |
| 27<br>**Pannonia**<br>*Planitia* | Low lying terrain in the centre of the map area. Several low mesas (*Sicilia* and *Corsica Mensa*), each a few kilometres across but only tens of metres high, comprise light-toned layered deposits beneath a thin cap of dark-toned, blocky material. |  |
| 28<br>**Raetia**<br>*Lacus* | Low elevation plain comprising a dark-toned surface to the west and a series of flat-topped, light-toned, layered, finger-like ridges to the east. Together, the ridges compose a fan-like landform that is associated with the termination of the North Neocoogoon Vallis. This fan-like feature is interpreted to be a delta. The western topographically low region connects northwards to *Aegyptus Vallis* and westwards to the *Narbonensis Palus*. |  |
| 29<br>**Tarraconesis**<br>*Terra* | Low elevation, light-toned plain in the far west of the region. The bright central area has a slightly higher elevation and is strongly associated with clay mineralogy detections (Quantin-Nataf et al., 2021). |  |
| 30<br>**Thracia**<br>*Palus* | Thracia Pallus is a low elevation zone that forms a several kilometer-wide trough-like valley that extends from *Aquitania Terra* in the east to *Germania Lacus* in the West. Remnants of a ridge run down-slope though the centre of the trough. |  |

**Table 4.** Data availability. The datasets used in this map are available through the ESA Guest Storage Facility (GSF) and the Open University Open Research Data Online (ORDO).

| Data set | Guest Storage Facility | Open University Open Research Data Online DOI |
|---|---|---|
| 01 Quad grid and regions | | |
| 01_a Quad Grid and Geographic regions | www.cosmos.esa.int/web/psa/psa_gsf | https://doi.org/10.21954/ou.rd.16451205.v1 |
| 02 CaSSIS | | |
| 02_a Georeferenced sRGB mosaic | www.cosmos.esa.int/web/psa/psa_gsf | https://doi.org/10.21954/ou.rd.16451217.v1 |
| 02_b Georeferenced sRGB images | www.cosmos.esa.int/web/psa/psa_gsf | https://doi.org/10.21954/ou.rd.16451217.v1 |
| 02_c Georeferenced cubes | www.cosmos.esa.int/web/psa/psa_gsf | https://doi.org/10.21954/ou.rd.16451217.v1 |
| 02_b All available cubes and sRGB images | www.cosmos.esa.int/web/psa/psa_gsf | Unavailable in this repository |
| 03 CTX DEM | | |
| 03_a CTX DEM Contours | www.cosmos.esa.int/web/psa/psa_gsf | https://doi.org/10.21954/ou.rd.16451220.v1 |
| 03_b CTX ORI Mosaic | www.cosmos.esa.int/web/psa/psa_gsf | https://doi.org/10.21954/ou.rd.16451220.v1 |
| 03_c CTX DEM Hill shade model | www.cosmos.esa.int/web/psa/psa_gsf | https://doi.org/10.21954/ou.rd.16451220.v1 |
| 03_d CTX DEM Mosaic | www.cosmos.esa.int/web/psa/psa_gsf | https://doi.org/10.21954/ou.rd.16451220.v1 |
| **Data set** | **Web link** | |
| HRSC MC11 mosaic tiles | http://hrscteam.dlr.de/HMC30/ | |
| HiRISE orthomosaic (and supporting CTX DEM mosaic) | https://doi.org/10.48326/idoc.psup.marssi.hirise.oxia<br>https://doi.org/10.48326/idoc.psup.marssi.ctx.oxia | |

### 3.3. Impact structures

A variety of impact structures at many stages of degradation occur in Oxia Planum (Roberts et al., 2021 *in review at JOM*; Figures 3 and 4). The overall physiography of the region suggests a quasi-circular basin. This is bounded to the northwest by the arcuate ridge in *Caledonia* and to the southeast by the high elevation plateau in *Noricum*. This could be a crypto impact basin (Figure 3 in Quantin-Nataf et al., 2021) comparable to larger quasi-circular depressions (QCD) in the northern lowland of Mars (Frey, 2006) or stealth QCD (Buczkowski, 2007). Many small impact craters have had their ejecta and rims removed, and most larger impact structures have experienced extensive erosion or inversion. Numerous small QCD, whose origin is unknown but are probably ancient, buried impact craters, are common in the north and central regions of the Oxia Basin (Figure 3).

### 3.4. Valleys and inverted channels

A variety of channels and valleys occur in Oxia Planum and have complex relationships with the regional geography (Figure 4(a,b)). The largest channels are *North*, *Central* and *South Neocoogoon Valles* in the southeast of the region, which incise *Noricum Promontorium* and *Aegyptus Vallis, which* crosscuts *Aegyptus Planitia* to terminate at dark materials in the low elevation *Dacia Palus*. The three *Neocoogoon Valles* are associated with Coogoon Valles, a ~10 km wide channel system east of the study area (Molina et al., 2017). *North* and *Central Neocoogoon Valles* are associated with sediment fans in *Raetia Palus* that formed after the phyllosilicate-bearing terrains (Quantin-Nataf et al., 2021). This leaves an open question about the relationship between the 10 km wide channel as part of the Coogoon Valles and the clay-bearing terrains in *Noricum*, *Cappadocia*, *Assyria* and *Aquitania* downslope of it.

Smaller channels (Figure 4(c,d)) occur in the light-toned clay-bearing terrains, and often as low relief valleys terminating in dark terrains (e.g. *Mesopotamia*). Several of these channels have narrow ridges in the upper reaches (e.g. *Lutetia Dorsum*) which are in continuum with channels in the lower reaches (e.g. *Lutetia Vallis*). These regions also have other evidence for an erosional environment, such as periodic bedrock ridges (Favaro et al., 2021; Silvestro et al., 2021), conducive to landscape inversion and inverted crater fill (Roberts et al., 2021 *in review at JOM*). This context suggests the ridges may be inverted channel deposits (Davis et al., 2016; Pain et al., 2007): ancient river beds exhumed from an alluvial landscape.

## 4 . Conclusions

This map and the associated data sets were created to provide a descriptive framework for the geography around Oxia Planum. These data will bridge the gap in scale between regional features (hundreds of square kilometres) and rover operations (hundreds of square metres) and support researchers investigating the ExoMars 2022 mission. They will be complemented by larger scale maps (thousands to tens of thousands square kilometres) which will be focussed on regional-scale stratigraphic relationships (Hauber et al., 2021).

From our observations about the geography, we present the following relationships and hypotheses. These serve as part of the ongoing multi-user mapping of the landing site so these data will be explored in future detailed investigations, and could be tested in-situ by observations and analyses made by instruments aboard the *Rosalind Franklin* rover:

- The overall topography suggests that Oxia Planum is a crypto impact basin, and the basement is a buried impact structure.

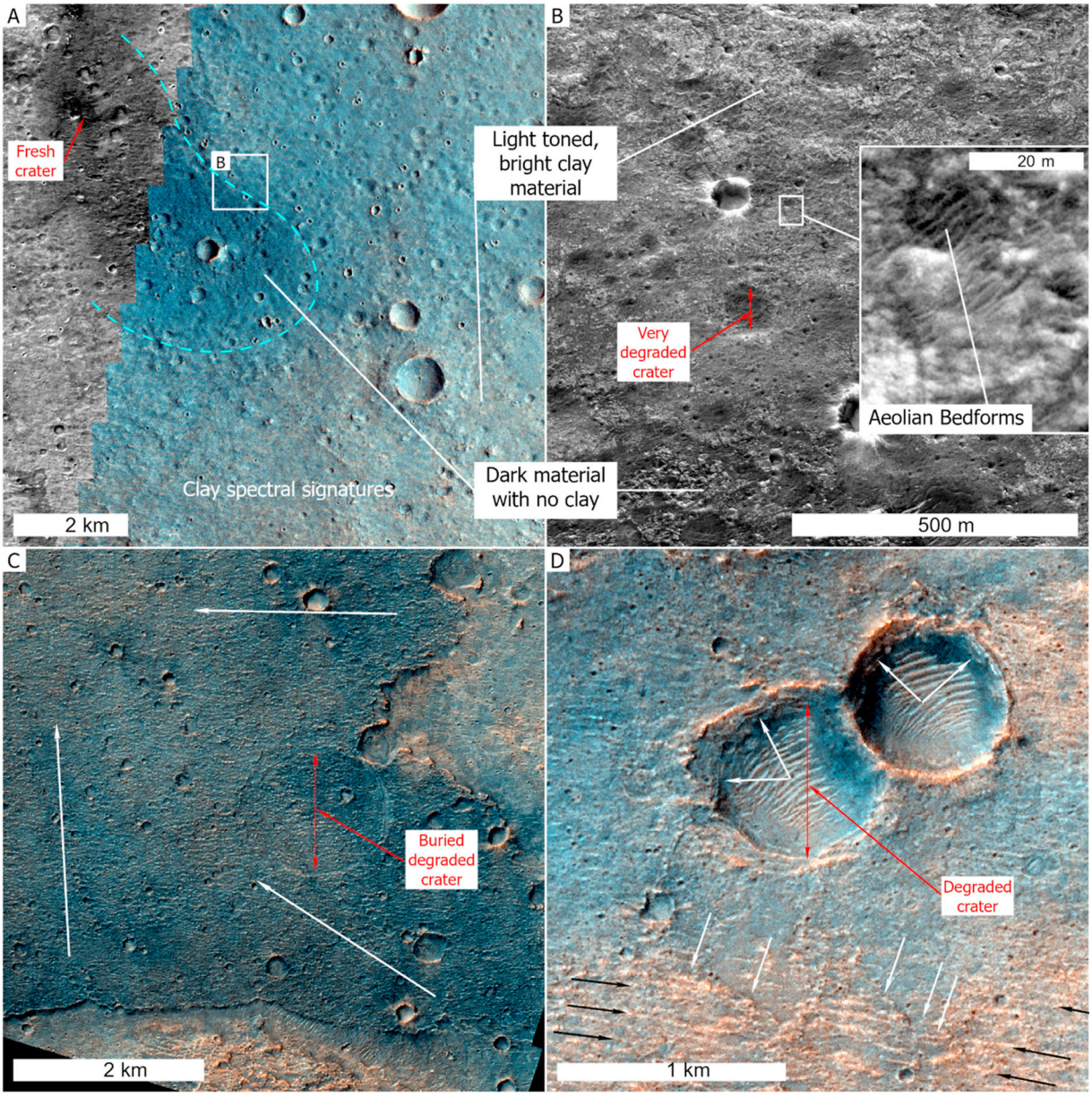



**Figure 3.** The surface of Oxia Planum. Examples of the different surfaces and impact structures (red) in Oxia Planum. (A) 'Blue' surfaces in CaSSIS synthetic colour images and dark surfaces in CTX ORI mosaic that anti-correlate with phyllosilicate detections (24.21W, 18.21N; MY35_006504_018_0_RGB; dashed cyan indicating the transition). (B) Very small aeolian bedforms cover the surface (HiRISE; ESP_048648_1985). (C) Dark toned material commonly occurs in low elevations or capping mesas (such as Germania Lacus; CaSSIS synthetic colour image; MY35_008742_019_0_RGB; 24.55W, 18.15N). Darker capping terrains are often light toned towards their centre (arrows) suggesting that the dark material is a thin layer or covering. (D) Bright terrains which correlate with phyllosilicate detections show evidence for layers or layering (as seen in the walls of these two craters) and are clearly seen even in 4 m/pixel CaSSIS data (image; MY35_009394_165_0_RGB; 24.36N, 18.01W) along with period bedrock ridges (Black arrows; e.g. Favaro et al., 2021). Note that the blue colour images represent mafic aeolian materials and the orange/white and yellow toned regions represent the clay-bearing bedrock materials (Parkes Bowen et al., 2021, in review).

- The variety of channels and their crosscutting relationships record several phases of fluvial activity.
- Widespread erosion has resulted in terrain inversion and exhumed an ancient alluvial landscape. Consequently, present-day local topographic highs may have been lows during deposition.
- The widespread presence of phyllosilicate-bearing deposits in this region implies the availability of liquid water in the entire area to alter the precursor deposits. However, it is not clear from this work how this may have come about.

## Data availability

The data used in the map, including the informal geographic areas and the Rover Operations Quad grid and multi band CaSSIS cubes being used for the scientific evaluation of Oxia Planum are freely available through the ESA Guest Storage Facility and the Open University Open Research Data Online (ORDO) (Table 4). A HiRISE orthomosaic and DEM (Quantin-Nataf et al., 2018; Volat & Quantan-Nataf, 2020) was produced for the high-resolution group mapping campaign of Oxia

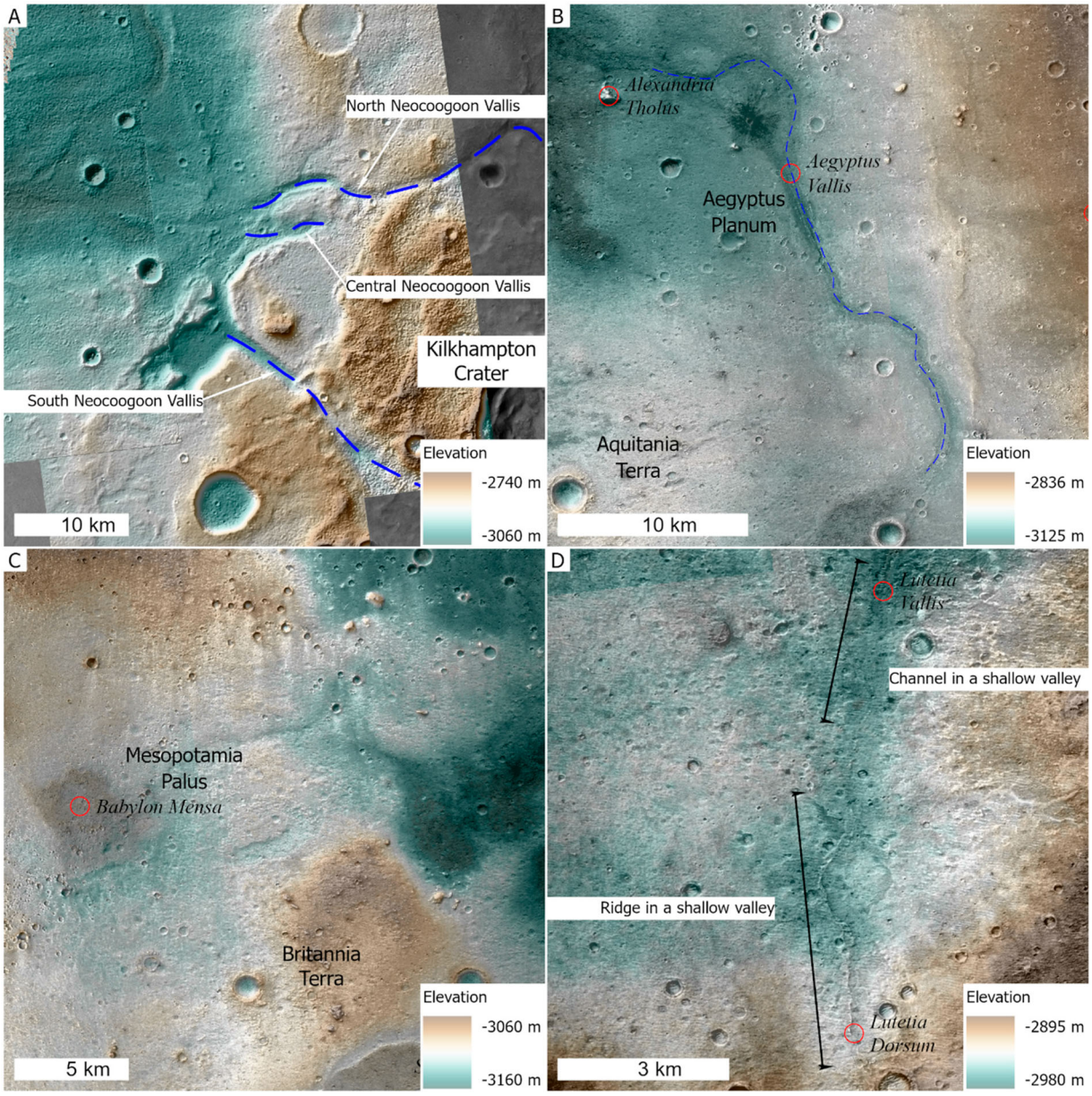



**Figure 4.** Valleys and inverted channels. The topography (green is low, brown is high) of valleys and channels in Oxia Planum with geographic locations highlighted with red circles. (A) The three channels associated with Coogoon Vallis in the south of Oxia Planum (at 23.74W, 17.74N), (B) Aegyptus Vallis, (at 24.04W, 18.20N) (C) The low relief valleys of Mesopotamia Palus (at 24.64W, 18.48N) and (D) the transition from narrow ridge to channel in a shallow inverted channel in the east of Lugdunensis (at 24.24W, 17.63N).

Planum (Sefton-Nash et al., 2020). That dataset was produced using the MarsSI infrastructure, is published on the Planetary SUrface Portal (PSUP), and is co-registered with the datasets presented here. We will update this database as new CaSSIS observations are obtained.

## Software

The map and other datasets were created and compiled in ESRI ArcPro 2.7. Creation of the CaSSIS RGB products were completed using ISIS3. CTX Digital Elevation Models and mosaicking of the CTX DEM used SocetSet® and Integrated Software for Images and Spectrometers (ISIS3). Georeferencing of CTX mosaic and CaSSIS data were conducted in ESRI ArcPro 2.7. CTX was mosaicked in the software Environment for Visualising Images (ENVI), with seamlines blended in Adobe Photoshop using the Avenza Geographic Imager extension. CaSSIS mosaic was created in ESRI ArcPro 2.7.

## Open Scholarship



This article has earned the Center for Open Science badges for Open Data and Open Materials through Open Practices Disclosure. The data and materials are openly accessible at and .

## Acknowledgements

We would like to acknowledge the following funding bodies, people and institutions to support this work. We thank NASA, the CTX camera team, and USGS for the CTX data and maintaining the ISIS and SOCET SET DEM workflows. The authors wish to thank the CaSSIS spacecraft and instrument engineering teams. CaSSIS is a project of the University of Bern and funded through the Swiss Space Office via ESA's PRODEX programme.

## Disclosure statement

No potential conflict of interest was reported by the author(s).

## Funding

We thank the UK space agency (UK SA) for funding P. Fawdon, on grants; ST/W002736/1, ST/R001413/1, and ST/R001413X/1 MRB on grants; ST/T002913/1, ST/V001965/1, ST/R001383/1, ST/R001413/1, P. Grindrod on grants; ST/L006456/1, ST/R002355/1, ST/V002678/1 and J. Davis on grant; ST/R002355/1 through the ongoing Aroura programme. The instrument hardware development was also supported by the Italian Space Agency (ASI) (ASI-INAF agreement no. I/2020-17-HH.0), INAF/Astronomical Observatory of Padova, and the Space Research Center (CBK) in Warsaw. Support from SGF (Budapest), the University of Arizona (Lunar and Planetary Lab.) and NASA are also gratefully acknowledged. Operations support from the UK Space Agency under grant ST/R003025/1 is also acknowledged.

## ORCID

*Peter Fawdon* http://orcid.org/0000-0003-1900-8347
*Peter Grindrod* http://orcid.org/0000-0002-0934-5131
*Csilla Orgel* http://orcid.org/0000-0001-7317-0092
*Elliot Sefton-Nash* http://orcid.org/0000-0002-5583-4438
*Solmaz Adeli* http://orcid.org/0000-0001-9972-409X
*Matt Balme* http://orcid.org/0000-0001-5871-7475
*Gabriele Cremonese* http://orcid.org/0000-0001-9021-1140
*Joel Davis* http://orcid.org/0000-0003-3522-7910
*Alessandro Frigeri* http://orcid.org/0000-0002-9140-3977
*Ernst Hauber* http://orcid.org/0000-0002-1375-304X
*Laetitia Le Deit* http://orcid.org/0000-0003-1361-5170
*Damien Loizeau* http://orcid.org/0000-0001-6001-3880
*Andrea Nass* http://orcid.org/0000-0001-7172-5170
*Adam Parks-Bowen* http://orcid.org/0000-0001-9838-9306
*Cathy Quantin-Nataf* http://orcid.org/0000-0002-8313-8595
*Nick Thomas* http://orcid.org/0000-0002-0146-0071
*Jorge L. Vago* http://orcid.org/0000-0003-1938-6639
*Matthieu Volat* http://orcid.org/0000-0002-5184-0304

## References

Anderson, R. C., Dohm, J. M., Golombek, M. P., Haldemann, A. F. C., Franklin, B. J., Tanaka, K. L., Kenneth, L., Lias, J., & Peer, B. (2001). Primary centers and secondary concentrations of tectonic activity through time in the western hemisphere of Mars. *Journal of Geophysical Research: Planets*, *106*(E9), 20563–20585. https://doi.org/10.1029/2000JE001278

Buczkowski, D. L. (2007). Stealth quasi-circular depressions (sQCDs) in the northern lowlands of Mars. *Journal of Geophysical Research*, *112*(E9). https://agupubs.onlinelibrary.wiley.com/action/showCitFormats?doi=10.1029%2F2006JE002836

Carter, J., Loizeau, D., Mangold, N., Poulet, F., & Bibring, J.-P. (2015). Widespread surface weathering on early Mars: A case for a warmer and wetter climate. *Icarus*, *248*(0), 373–382. https://doi.org/10.1016/j.icarus.2014.11.011

Cook, A. C., Oberst, J., Roatsch, T., Jaumann, R., & Acton, C. (1996). Clementine imagery: Selenographic coverage for cartographic and scientific use. *Planetary and Space Science*, *44*(10), 1135–1148. https://doi.org/10.1016/S0032-0633(96)00061-X

Davis, J. M., Balme, M. R., Grindrod, P. M., Williams, R. M. E., & Gupta, S. (2016). *Inverted Channels in Arabia Terra, Mars: Remnants of and ancients drainge network* (p. #1982) [Paper presentation] At the 47th Lunar and Planetary Science Conference (2016), Abstract #1982, 47th Lunar and Planetary Science Conference, The Woodlands, TX. http://www.hou.usra.edu/meetings/lpsc2016/pdf/1982.pdf

Dickeson, Z. I., & Davis, J. M. (2020). Martian oceans. *Astronomy & Geophysics*, *61*(3), 3.11–3.17. https://doi.org/10.1093/astrogeo/ataa038

ESA, & The ExoMars 2018 Landing Site Selection Working Group (LSSWG). (2014, September 2). *ESA - Robotic Exploration of Mars: Recommendation for the narrowing of ExoMars 2018 landing sites*. Retrieved May 27, 2015, from http://exploration.esa.int/mars/54707-recommendation-for-the-narrowing-of-exomars-2018-landing-sitesrecommendation-for-the-narrowing-of-exomars-2018-landing-sites/#

Esri. (2020). *How spline works*. https://pro.arcgis.com/en/pro-app/latest/tool-reference/3d-analyst/how-spline-works.htm

Esri. (2021). *Grid index features*. https://pro.arcgis.com/en/pro-app/latest/tool-reference/cartography/grid-index-features.htm

Favaro, E. A., Balme, M. R., Davis, J. M., Grindrod, P. M., Fawdon, P., Barrett, A. M., & Lewis, S. R. (2021). The aeolian environment of the landing site for the ExoMars Rosalind Franklin rover in Oxia planum. *Mars. Journal of Geophysical Research: Planets*, *126*(4), 2020JE006723. https://doi.org/10.1029/2020JE006723

Fawdon, P., Balme, M. R., Bridges, J., Davis, J. M., Gupta, S., & Quantan-Nataf, C. (2021). *Rivers and lakes in Western Arabia Terra: The fluvial catchment of the ExoMars 2022 rover landing site. Earth and Space Science Open Archive*, *47*. https://doi.org/10.1002/essoar.10507896.1

Fawdon, P., Roberts, A. L., & Mirino, M. M. (2020, March 16th-20th). *Impact crater degradation and The timing of resurfacing events in Oxia planum*. In Proceedings of the 51th Lunar and Planetary Science Conference (p. #2240). http://www.lpi.usra.edu/meetings/lpsc2020/pdf/2240.pdf

Frey, H. V. (2006). Impact constraints on, and a chronology for, major events in early Mars history. *Journal of Geophysical Research*, *111*(E8), https://doi.org/10.1029/2005JE002449

Gary-Bicas, C. E., & Rogers, A. D. (2021). Geologic and thermal characterization of Oxia Planum using Mars odyssey THEMIS data. *Journal of Geophysical Research:*

*Planets*, *126*(2), e2020JE006678. https://doi.org/10.1029/2020JE006678

Gwinner, K., Jaumann, R., Hauber, E., Hoffmann, H., Heipke, C., Oberst, J., Neukum, G., Ansan, V., Bostelmann, J., Dumke, A., Elgner, S., Erkeling, G., Fueten, F., Hiesinger, H., Hoekzema, N.M., Kersten, E., Loizeau, D., Matz, K.-D., McGuire, P.C., … Willner, K. (2016). The high Resolution Stereo Camera (HRSC) of Mars Express and its approach to science analysis and mapping for Mars and its satellites. *Planetary and Space Science*, *126*, 93–138. https://doi.org/10.1016/j.pss.2016.02.014

Hartmann, W. K., & Neukum, G. (2001). Cratering chronology and the evolution of Mars. *Space Science Reviews*, *96*(1), 165–194. https://doi.org/10.1023/a:1011945222010

Hauber, E., Tirsch, D., Adeli, S., Acktories, S., Steffens, S., Nass, A., & Rsowg, E. (2021, March 15th-19th). *Regional geologic mapping of the Oxia Planum landing site for the exomars 2022 mission* (p. 2057) [Paper presentation]. At the Lunar and Planetary Science Conference.

Howington-Kraus, E., Kirk, R., Soderblom, L., Giese, B., & Oberst, J. (2002). USGS and DLR topographic mapping of comet Borrelly. *International Archives of Photogrammetry Remote Sensing and Spatial Information Sciences*, *34*(4), 723–727. http://pubs.er.usgs.gov/publication/70201649

IAU. (1979). *Gazetteer of planetary nomenclature*. Retrieved June 5, 2020, from https://planetarynames.wr.usgs.gov/DescriptorTerms

Kersten, E., Gwinner, K., Michael, G., Bostelmann, J., Dumke, A., Wählisch, M., & Jaumann, R. (2018). *Topographic mapping of the Mars MC quadrangles using HRSC data*, EPSC2018-352.

Kirk, R., Howington-Kraus, E., Redding, B., Galuszka, D., Hare, T. M., Archinal, B. A., Soderblom, L. A., & Barrett, J. M. (2003). High-resolution topomapping of candidate MER landing sites with Mars Orbiter Camera narrow-angle images. *Journal of Geophysical Research: Planets*, *108*(E12), 148–227. https://doi.org/10.1029/2003JE002131

Kirk, R., Howington-Kraus, E., Rosiek, M. R., Anderson, J. A., Archinal, B. A., Becker, K. J., Cook, D. A., Galuszka, D. M., Geissler, P. E., Hare, T. M., Holmberg, I. M., Keszthelyi, L. P., Redding, B. L., Delamere, W. A., Gallagher, D., Chapel, J. D., Eliason, E. M., King, R., & McEwen, A. S. (2008). Ultrahigh resolution topographic mapping of Mars with MRO HiRISE stereo images: Meter-scale slopes of candidate Phoenix landing sites. *Journal of Geophysical Research*, *113*(E3), E00A24. https://doi.org/10.1029/2007JE003000

Kirk, R. L., Howington-Kraus, E., Hare, T., Dorrer, E., Cook, D., Becker, K., Thompson, K., Redding, B., Blue, J., Galuszka, D., Lee, E. M., Gaddis, L. R., Johnson, J. R., Soderblom, L. A., Ward, A. W., Smith, P. H., & Britt, D. T. (1999). Digital photogrammetric analysis of the IMP camera images: Mapping the Mars Pathfinder landing site in three dimensions. *Journal of Geophysical Research: Planets*, *104*(E4), 8869–8887. https://doi.org/10.1029/1998JE900012

Malin, M. C., Bell, J. F. III, Cantor, B. A., Caplinger, M. A., Calvin, W. M., Clancy, R. T., Edgett, K. S., Edwards, L., Haberle, R. M., James, P. B., Lee, S. W., Ravine, M. A., Thomas, P. C., & Wolff, M. J. (2007). Context Camera investigation on board the Mars Reconnaissance Orbiter. *Journal of Geophysical Research*, *112*(E5), E05S04. https://doi.org/10.1029/2006je002808

Mandon, L., Parkes Bowen, A., Quantin-Nataf, C., Bridges, J. C., Carter, J., Pan, L., Beck, P., Dehouck, E., Volat, M., Thomas, N., Cremonese, G., Tornabene, L. L., & Thollot, P. (2021). Morphological and spectral diversity of the clay-bearing unit at the ExoMars landing site Oxia Planum. *Astrobiology*, *21*(4), 464–480. https://doi.org/10.1089/ast.2020.2292

McNeil, J. D., Fawdon, P., Balme, M. R., & Coe, A. L. (2021). Morphology, morphometry and distribution of isolated landforms in southern Chryse Planitia, Mars. *Journal of Geophysical Research: Planets*, *126*(5), e2020JE006775. https://doi.org/10.1029/2020JE006775

Michalski, J. R., & Bleacher, J. E. (2013). Supervolcanoes within an ancient volcanic province in Arabia Terra, Mars. *Nature*, *502*(7469), 47–52. https://doi.org/10.1038/nature12482

Molina, A., López, I., Prieto-Ballesteros, O., Fernández-Remolar, D., de Pablo, MÁ, & Gómez, F. (2017). Coogoon Valles, western Arabia Terra: Hydrological evolution of a complex Martian channel system. *Icarus*, *293*, 27–44. https://doi.org/10.1016/j.icarus.2017.04.002

Neukum, G., Jaumann, R.. (2004). HRSC: The high resolution stereo camera on Mars express. In A. Wilson (Ed.), *Mars express : The scientific payload*. ESA-SP. ESA. https://elib.dlr.de/11065/

Noe Dobrea, E. Z., Bishop, J. L., McKeown, N. K., Fu, R., Rossi, C. M., Michalski, J. R., Heinlein, C., Hanus, V., Poulet, F., Mustard, R. J. F., Murchie, S., McEwen, A. S., Swayze, G., Bibring, J.-P., Malaret, E., & Hash, C. (2010). Mineralogy and stratigraphy of phyllosilicate-bearing and dark mantling units in the greater Mawrth Vallis/west Arabia Terra area: Constraints on geological origin. *Journal of Geophysical Research*, *115*(E7). https://agupubs.onlinelibrary.wiley.com/action/showCitFormats?doi=10.1029%2F2009JE003351

Pain, C. F., Clarke, J. D. A., & Thomas, M. (2007). Inversion of relief on Mars. *Icarus*, *190*(2), 478–491. https://doi.org/10.1016/j.icarus.2007.03.017

Pan, L., Quantin-Nataf, C., Breton, S., & Michaut, C. (2019). The impact origin and evolution of Chryse Planitia on Mars revealed by buried craters. *Nature Communications*, *10*(1), 4257. https://doi.org/10.1038/s41467-019-12162-0

Parkes Bowen, A., Bridges, J., Tornabene, L., Mandon, L., Quantin-Nataf, C., Patel, M., Thomas, N., & Cremonese, G. (2021). A CaSSIS and HiRISE Map of the clay-bearing units at the ExoMars2022 landing site in Oxia Planum. *Planetary and Space Science In review at Planetary and Space Sciences*.

Quantin-Nataf, C., Carter, J., Mandon, L., Thollot, P., Balme, M., Volat, M., Pan, L., Loizeau, D., Millot, C., Breton, S., Dehouck, E., Fawdon, P., Gupta, S., Davis, J., Grindrod, P. M., Pacifici, A., Bultel, B., Allemand, P., Ody, A., … Broyer, J. (2021). Oxia Planum: The landing site for the ExoMars "Rosalind Franklin" Rover Mission: Geological Context and prelanding interpretation. *Astrobiology*, *21*(3), 345–366. https://doi.org/10.1089/ast.2019.2191

Quantin-Nataf, C., Lozac'h, L., Thollot, P., Loizeau, D., Bultel, B., Fernando, J., Allemand, P., Dubuffet, F., Poulet, F., Ody, A., Clenet, H., Leyrat, C., & Harrison, S. (2018). MarsSI: Martian surface data processing information system. *Planetary and Space Science*, *150*, 157–170. https://doi.org/10.1016/j.pss.2017.09.014

Roberts, A. L., Fawdon, P., & Mirino, M. (2021). Impact crater degradation, Oxia Planum, Mars. *Journal of Maps*, *17*(2), 569–578. https://doi.org/10.1080/17445647.2021.1976685

Sefton-Nash, E., Balme, M., Quantin-Nataf, C., Fawdon, P., Volat, M., Hauber, E., Orgel, C., Frigeri, A., Le Deit, L., Ruesch, O., Adeli, S., Loizeau, D., Davis, J., Grindrod, P., Nass, A., de Witte, S., Calef, F. J., & Soliman, T. K. (2020). *HiRISE-scale characterization of the Oxia Planum landing site for the ExoMars 2022 mission* (pp. EPSC2020-978) [Paper presentation]. *At the European Planetary Science Congress.* https://doi.org/10.5194/epsc2020-978

Silvestro, S., Pacifici, A., Salese, F., Vaz, D. A., Neesemann, A., Tirsch, D., Popa, C.I., Pajola, M., Franzese, G., Mongelluzzo, G., Ruggeri, A.C., Cozzolino, F., Porto, C., & Esposito, F. (2021). Periodic bedrock ridges at the ExoMars 2022 landing site: Evidence for a changing wind regime. *Geophysical Research Letters*, *48*(4), e2020GL091651. https://doi.org/10.1029/2020GL091651

Smith, D. E., Zuber, M. T., Frey, H. V., Garvin, J. B., Head, J. W., Muhleman, D. O., Pettengill, G. H., Phillips, R. J., Solomon, S. C., Zwally, H. J. , Banerdt, W. B., Duxbury, T. C., Golombek, M. P. , Lemoine, F. G., Neumann, G. A. , Rowlands, D. D., Aharonson, O., Ford, P. G., Ivanov, A. B., … Sun, X. (2001). Mars Orbiter Laser Altimeter: Experiment summary after the first year of global mapping of Mars. *Journal of Geophysical Research: Planets*, *106*(E10), 23689–23722. https://doi.org/10.1029/2000je001364

Tanaka, K. L., Robbins, S. J., Fortezzo, C. M., Skinner, J. A., & Hare, T. M. (2014a). The digital global geologic map of mars: Chronostratigraphic ages, topographic and crater morphologic characteristics, and updated resurfacing history. *Planetary and Space Science*, *95*, 11–24. https://doi.org/10.1016/j.pss.2013.03.006

Tanaka, K. L., Skinner, J. A., Dohm, J., Irwin III, R. P., Kolb, E. J., Fortezzo, C. M., Platz, T., Michael, G. G., & Hare, T. M. (2014). Geologic map of Mars: U.S. geological survey scientific investigations map 3292, Scale 1:20,000,000, Pamphlet 43 p. http://pubs.usgs.gov/sim/3292/

Thomas, N., Cremonese, G., Ziethe, R., Gerber, M., Brändli, M., Bruno, G., Erismann, M., Gambicorti, L., Gerber, T., Ghose, K., Gruber, M., Gubler, P., Mischler, H., Jost, J., Piazza, D., Pommerol, A., Rieder, M., Roloff, V., Servonet, A., … Wray, J. J. (2017). The Colour and Stereo Surface Imaging System (CaSSIS) for the ExoMars Trace Gas Orbiter. *Space Science Reviews*, *212*(3), 1897–1944. https://doi.org/10.1007/s11214-017-0421-1

Tornabene, L. L., Seelos, F. P., Pommerol, A., Thomas, N., Caudill, C. M., Becerra, P., Bridges, J. C., Byrne, S., Cardinale, M., Chojnacki, M., Conway, S. J., Cremonese, G., Dundas, C. M., El-Maarry, M. R., Fernando, J., Hansen, C. J., Hansen, K., Harrison, T. N., Henson, R., … Wray, J. J. (2017). Image simulation and assessment of the colour and spatial capabilities of the Colour and Stereo Surface Imaging System (CaSSIS) on the ExoMars Trace Gas Orbiter. *Space Science Reviews*, *214*(1), 18. https://doi.org/10.1007/s11214-017-0436-7

USGS, & MRCTR GIS Lab. (2018, September 7). *Standard operating procedures for creating contours from high-resolution digital terrain models (DTM) with ArcMap 10.3.* https://astropedia.astrogeology.usgs.gov/alfresco/d/d/workspace/SpacesStore/2293baf7-64aa-4a8f-8782-b0cce41bc36e/PGM_GIS_SOP_Contours_170420.pdf

Vago, J. L., Spoto, F., & Bauer, M. (2018, September 11). *Oxia Planum favoured for ExoMars surface mission.* https://exploration.esa.int/web/mars/-/60914-oxia-planum-favoured-for-exomars-surface-mission

Vago, J. L., Westall, F., Coates, A. J., Jaumann, R., Korablev, O., Ciarletti, V., Mitrofanov, I., Josset, J.-L., De Sanctis, M. C., Bibring, J.-P., Rull, F., Goesmann, F., Steininger, H., Goetz, W., Brinckerhoff, W., Szopa, C., Raulin, F., Edwards, H. G. M., Whyte, L. G., … and the ExoMars Project Team (2017). Habitability on early Mars and the search for biosignatures with the ExoMars rover. *Astrobiology*, *17*(6–7), 471–510. https://doi.org/10.1089/ast.2016.1533

Volat, M., & Quantan-Nataf, C. (2020). *Oxia HiRISE DEM mosaic.* https://doi.org/10.48326/idoc.psup.marssi.hirise.oxia